

Lyophilized Scaffolds Fabricated from 3D-Printed Photocurable Natural Hydrogel for Cartilage Regeneration

Huitang Xia,^{†,‡,§,§} Dandan Zhao,^{†,‡,§,§} Hailin Zhu,^{||,⊥,§} Yujie Hua,^{×,§} Kaiyan Xiao,^{†,§} Yong Xu,[#] Yanqun Liu,^{‡,§} Weiming Chen,^{†,§} Yu Liu,[§] Wenjie Zhang,^{†,§} Wei Liu,^{†,§} Shengjian Tang,^{‡,§} Yilin Cao,^{†,§} Xiaoyun Wang,^{*,⊗} Harry Huimin Chen,^{*,||,⊥} and Guangdong Zhou^{*,†,‡,§,§}

[†]Department of Plastic and Reconstructive Surgery, Shanghai Ninth People's Hospital, Shanghai Jiao Tong University School of Medicine, Shanghai Key Laboratory of Tissue Engineering, Shanghai, P.R. China 200011

[‡]Research Institute of Plastic Surgery, Wei Fang Medical College, Wei Fang, Shandong P.R. China

[§]National Tissue Engineering Center of China, Shanghai, P.R. China

^{||}StemEasy Biotech, Ltd., BridgeBio Park, Jiangyin, Jiangsu 214434, P.R. China

[⊥]State Key Laboratory of Biotherapy, Sichuan University, Chengdu, Sichuan 610041, P. R. China

[#]Department of Thoracic Surgery, Shanghai Pulmonary Hospital, Tongji University School of Medicine, Shanghai, P.R. China

[⊗]Minhang Branch of Yueyang Hospital of Integrative Chinese & Western Medicine Affiliated to Shanghai University of Traditional Chinese Medicine, Shanghai, P.R. China

[×]Key Laboratory for Advanced Materials Institute of Fine Chemicals East China University of Science and Technology, 130 Meilong Road, Shanghai 200237, P.R. China



ABSTRACT: Repair of cartilage defects is highly challenging in clinical treatment. Tissue engineering provides a promising approach for cartilage regeneration and repair. As a core component of tissue engineering, scaffolds have a crucial influence on cartilage regeneration, especially in immunocompetent large animal and human. Native polymers, such as gelatin and hyaluronic acid, have known as ideal biomimetic scaffold sources for cartilage regeneration. However, how to precisely control their structure, degradation rate, and mechanical properties suitable for cartilage regeneration remains a great challenge. To address these issues, a series of strategies were introduced in the current study to optimize the scaffold fabrication. First, gelatin and hyaluronic acid were prepared into a hydrogel and 3D printing was adopted to ensure precise control in both the outer 3D shape and internal pore structure. Second, methacrylic anhydride and a photoinitiator were introduced into the hydrogel system to make the material photocurable during 3D printing. Finally, lyophilization was used to further enhance mechanical properties and prolong degradation time. According to the current results, by integrating photocuring 3D printing and lyophilization techniques, gelatin and hyaluronic acid were successfully fabricated into human ear- and nose-shaped scaffolds, and both scaffolds achieved shape similarity levels over 90% compared with the original digital models. The scaffolds with 50% infill density achieved proper internal pore structure suitable for cell distribution, adhesion, and proliferation. Besides, lyophilization further enhanced mechanical strength of the 3D-printed hydrogel and slowed its degradation rate matching to cartilage regeneration. Most importantly, the scaffolds combined with chondrocytes successfully regenerated mature cartilage with typical lacunae structure and cartilage-specific extracellular matrixes both *in vitro* and in the autologous goat model. The current study established novel scaffold-fabricated strategies for native polymers and provided a novel natural 3D scaffold

continued...

Received: July 1, 2018

Accepted: August 29, 2018

Published: August 29, 2018

with satisfactory outer shape, pore structure, mechanical strength, degradation rate, and weak immunogenicity for cartilage regeneration.

KEYWORDS: photocuring, 3D printing, native polymers, cartilage regeneration, lyophilization, scaffold, gelatin, hyaluronic acid

1. INTRODUCTION

Cartilage has a poor intrinsic self-repair capacity owing to its avascular and aneural nature.^{1,2} Consequently, cartilage repair is highly challenging in clinical treatment. Tissue engineering provides a promising approach for cartilage regeneration and repair.^{3,4} As a core component of the tissue engineering process, scaffolds elicit a crucial influence on stabilizing cartilage regeneration, especially in immunocompetent large animal models.^{5–7} However, development of a structurally and functionally optimized scaffold remains a challenge in cartilage regeneration at present.

Material source is a primary factor for cartilage regeneration, owing to its pivotal role in ensuring biocompatibility and mechanical strength. Scaffold materials predominantly include synthetic and natural polymers, depending on their origin. Synthetic polymers have many advantages suitable for cartilage regeneration, such as ease of processing, high mechanical properties, and controllability in shape, porous structure, and degradation rate.^{8–10} However, synthetic materials also have properties unfavorable for cartilage regeneration, such as inferior biocompatibility, low bioactivity, and aseptic inflammation caused by their degradation products when implanted into immunocompetent large animal models and humans. Consequently, synthetic polymers are not the ideal choice for cartilage regeneration. Conversely, natural polymers with superior biocompatibility, good biological activity, low immunogenicity, and low cytotoxicity from their degradation products have become favorable as biomimetic scaffolds for cartilage regeneration.^{11,12} Two key native polymers, collagen and hyaluronic acid, have been widely used for cartilage regeneration.^{13–15} However, current scaffolds based on these polymers have not achieved satisfactory cartilage regeneration because of the following drawbacks: (i) imprecise control in the outer three-dimensional (3D) shape and internal pore structure; (ii) excessive degradation rate mismatch to cartilage regeneration; (iii) inferior mechanical strength failing to maintain the original 3D shape.^{16–18}

To address these issues, we proposed a series of strategies to optimize the fabrication procedures of porous scaffolds based on collagen and hyaluronic acid. First, gelatin (a derivative of collagen) and hyaluronic acid were prepared into a hydrogel and 3D printing was adopted to ensure precise control in both the outer 3D shape and internal pore structure.^{19,20} Second, methacrylic anhydride and a photoinitiator were introduced into the hydrogel system to make the material photocurable, thus further promoting precision of the hydrogel structure through a photo-cross-linking reaction during 3D printing.^{21,22} Simultaneously, the photo-cross-linking reaction significantly enhanced mechanical strength of the 3D-printed hydrogel and slowed its degradation rate. Finally, lyophilization was used to further enhance the mechanical properties of the 3D-printed hydrogel scaffolds and transform them into solid scaffolds, which also contributed to slowing the degradation rate and improving the operability of cell-seeding.

By integrating these aforementioned strategies into our current study, we hypothesized that we could create a structurally and functionally-optimized porous scaffold with precise structural control, an optimal degradation rate matched to

native cartilage regeneration, and satisfactory mechanical strength. The photo-cross-linkable hydrogel was prepared using gelatin and hyaluronic acid, thus fabricated into porous scaffolds with precise outer 3D shapes (representative of a human ear and nose) and a satisfactory internal pore structure, using photocuring 3D printing and lyophilization technologies. After testing their characterization and biocompatibility, chondrocytes were seeded into the scaffolds to evaluate the feasibility of cartilage regeneration both *in vitro* and *in vivo*. The current study provides a series of strategies for porous scaffold fabrication based on native polymers and a novel natural biodegradable scaffold for cartilage regeneration.

2. MATERIALS AND METHODS

2.1. Scaffold Preparation Using Photocuring 3D Printing and Lyophilization.

2.1.1. Macromer Synthesis and Preparation of Photo-Cross-Linkable Hydrogel. Gelatin-methacrylamide (GelMA) and hyaluronic acid methacrylate (HAMA) were synthesized based on previously published protocols,^{23,24} respectively. GelMA (5%), HAMA (2%), and the photoinitiator (lithium phenyl-2,4,6-trimethylbenzoyl-phosphinate, LAP, 0.5%, w/v) were dissolved in deionized water at 60 °C to form a photo-cross-linkable hydrogel. The final hydrogel was stored at 4 °C in the dark for subsequent use.

2.1.2. Characterization of Macromers and Photocuring Hydrogel.

The structures of all above macromers, gel precursor, and photocuring hydrogel were characterized by and compared with a ¹H NMR experiment. ¹H NMR spectra was recorded on a Bruker 400 MHz NMR spectrometer. Chemical shifts were reported in parts per million (ppm).

The viscosity and shear-thinning behavior of the gel precursor was tested to evaluate its printability as the bioink. Rheological analysis was used to evaluate the photocuring performance of gel precursor. These experiments were performed on HAAKE MARS Rotational Rheometer with parallel-plate (P20 TiL, 20 mm diameter) geometry at 25 °C. Shear-thinning behavior was performed at a 0.5 mm gap from 0 to 100 1/s. Dynamic rheology experiments were exposed to blue light (405 nm, 30 mW cm²). Time sweep oscillatory test was performed at a 10% strain (CD mode), 1 Hz frequency, and a 0.5 mm gap for 120 s. The gel point was determined as the time when the storage modulus (*G'*) surpassed the loss modulus (*G''*).

2.1.3. Scaffold Fabrication with Photocuring 3D Printing and Lyophilization.

The bioprinting system used in the current study was a desktop pneumatic extrusion-based bioprinter (BioBots Beta, USA) with a 405 nm blue light. To construct the 3D-printed hydrogels, infill density was set as either 30%, 50%, or 70%. Each layer height was set as 0.1 mm and deposited at a 90° angle to the underlying layer. During the printing process, the photo-cross-linkable hydrogel was solidified under constant irradiation from the blue light source. After 3D printing, the scaffolds were frozen at –80 °C for 4 h and lyophilized for 48 h. The scaffolds were sterilized with ethylene oxide for subsequent use.

The 3D digital ear- and nose-shaped models were established as previously described.²⁵ Both ear- and nose-shaped scaffolds were prepared based on the digital models by photocuring 3D printing and lyophilization, as referred to in the aforementioned methods. A 3D laser scanning system was used for the shape analysis as previously described.²⁵

2.2. Characterization and Biocompatibility Evaluation of 3D Scaffolds.

2.2.1. Morphology and Porosity of 3D Scaffolds. The surface morphology and pore structure of the scaffolds were examined by scanning electron microscopy (SEM). Scaffold pore size at different infill densities was measured according to SEM.

2.2.2. Cell Seeding Efficiency and Viability in the Scaffold. Goat auricular cartilage-derived chondrocytes were isolated and cultured as previously described.²⁶ Chondrocytes were seeded into the scaffolds at a concentration of 90 × 10⁶ cells per milliliter (the concentration of cell

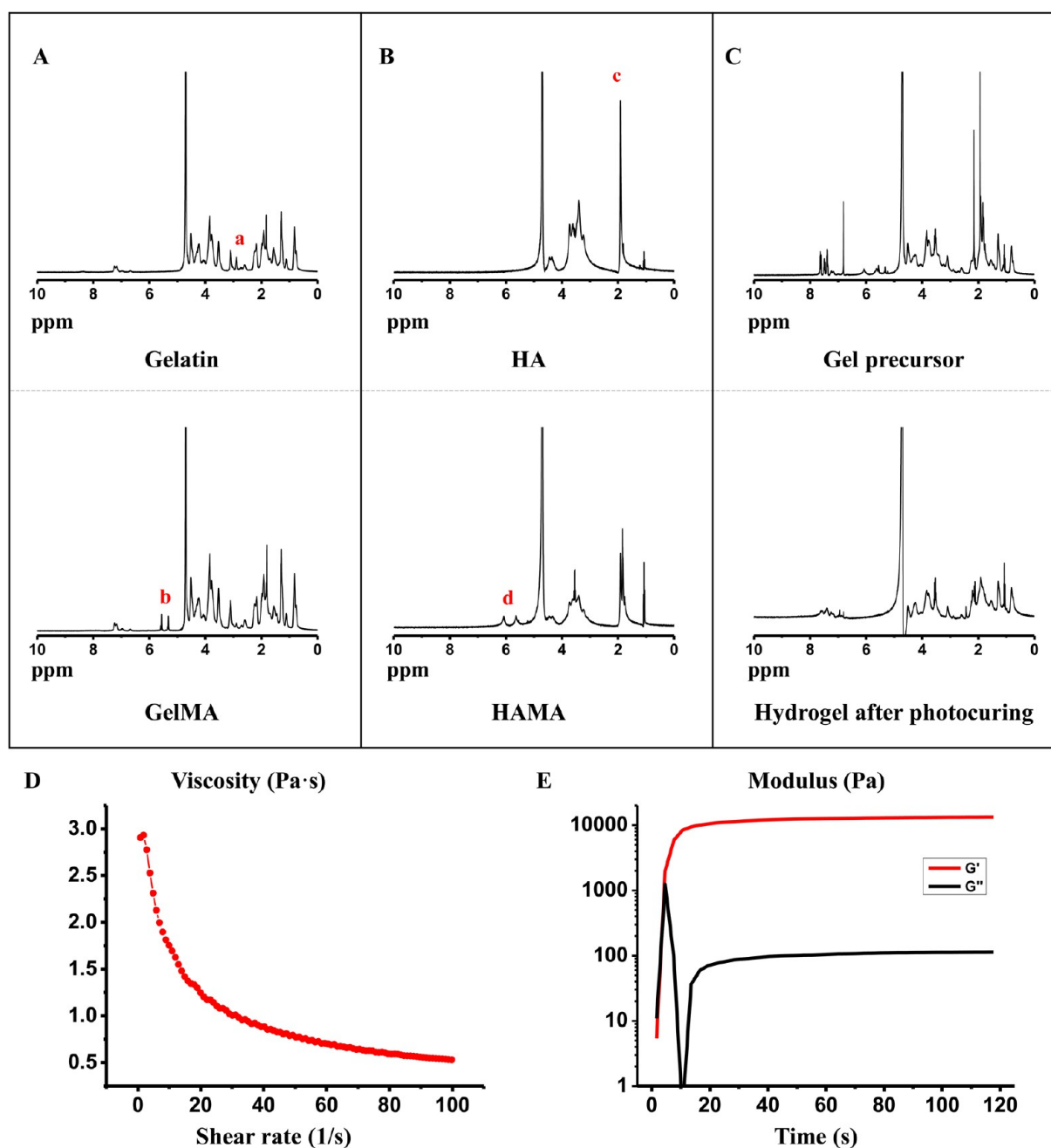


Figure 2. Characterization of macromers, gel precursor, and photocuring hydrogel. (A) Characterization of methacrylate-modified gelatin (GelMA). The lysine signal of the gelatin reduced at 2.9 ppm (a) and the methacrylamide vinyl group signal increased at 5.4 and 5.6 ppm (b), indicating successful MA modification of the gelatin. (B) Characterization of methacrylate-modified hyaluronic acid (HAMA). The *N*-acetyl glucosamine signal of hyaluronic acid reduced at 1.9 ppm (c) and the methacrylamide vinyl group signal increased at 5.6 and 6.1 ppm (d), indicating successful MA modification of hyaluronic acid. (C) The ^1H NMR trace of the photo-cross-linking process of the gel precursor. The signals of the gel precursor distinctly decreased at 1.8–2.5 ppm and 5.4–7.8 ppm, indicating successful polymerization of GelMA and HAMA. (D) The viscosity and shear-thinning behavior of the gel precursor. The viscosity of gel precursor based on GelMA and HAMA decreased as the shear rate increased which indicated its extrudable property and good printability as the bioink. (E) Rheology analysis shows the hydrogel formation and fast gelation at approximately 4 s upon 405 nm blue light.

2.6. *In Vitro* Cartilage Regeneration and *In Vivo* Implantation.

The chondrocyte–scaffold constructs were cultured in chondrogenic medium for 2, 4, and 8 weeks for *in vitro* cartilage regeneration and then subcutaneously implanted into nude mice for another 8 weeks. Some of the 2-week *in vitro* samples were subcutaneously implanted into an autologous goat for another 8 weeks. All *in vitro* and *in vivo* samples were harvested for cartilage regeneration evaluation.

Nude mice and goats were purchased from Shanghai Jiagan Experimental Animal Raising Farm (Shanghai, China). The Animal

Care and Use Committee of Shanghai Jiao Tong University School of Medicine approved all the animal studies for this research.

2.7. Histological Evaluation of Regenerated Cartilage.

The samples were fixed in 4% paraformaldehyde, embedded in paraffin, and sectioned for histological and immunohistochemical analysis. Sections were stained according to previously established methods with hematoxylin and eosin (HE), Safranin-O, and type II collagen to evaluate histological structure and cartilage ECM deposition in the regenerated cartilage.³²

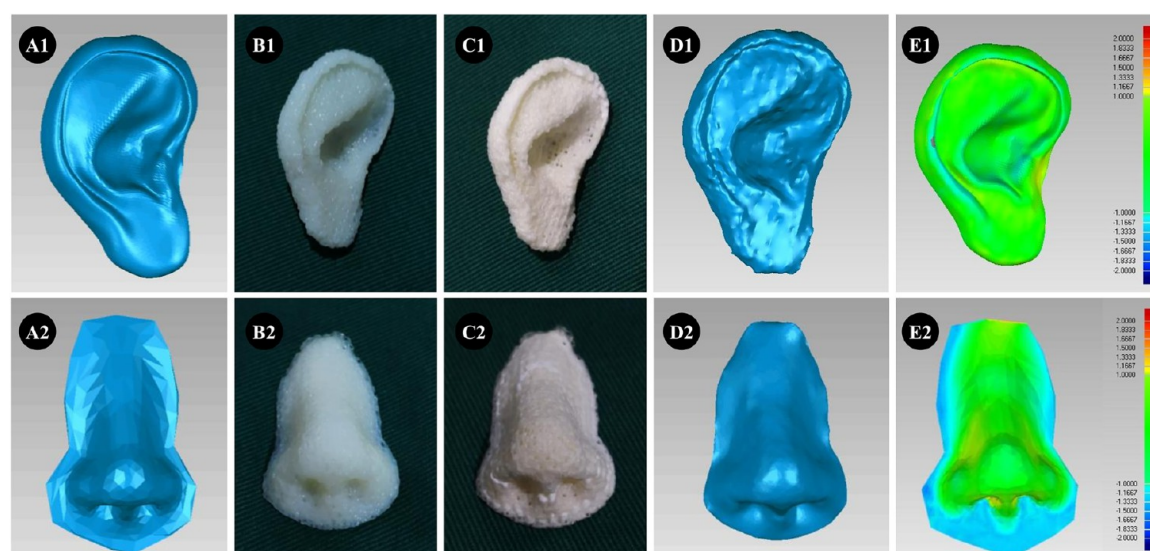


Figure 3. Preparation of human ear- and nose-shaped scaffolds and shape analysis: (A1, A2) original digital models; (B1, B2) 3D-printed hydrogel; (C1, C2) scaffolds after lyophilization; (D1, D2) laser scan images of the lyophilized scaffolds; (E1, E2) shape similarity of the scaffolds compared with the digital models (similarity of ear- and nose-shaped scaffolds reaches 98% and 93%, respectively).

2.8. Biomechanical and Biochemical Evaluations. Young's modulus of the samples was detected and analyzed according to the slope of the stress–strain curve as previously described to evaluate the mechanical properties of the regenerated cartilage. The samples were collected and minced to conduct cartilage-related biochemical evaluations for glycosaminoglycan (GAG), total collagen, and DNA quantifications,^{33,34} quantified by the dimethylmethylene blue assay (DMMB, Sigma-Aldrich, USA), hydroxyproline assay kit (Sigma-Aldrich, USA), and PicoGreen dsDNA assay (Invitrogen, USA), respectively.

2.9. Statistical Analysis. All quantitative data are shown as means \pm standard deviation. Upon confirmation of normal data distribution, one-way analysis of variance and the posthoc least significant difference test were used to determine statistical significance among groups. A p value less than 0.05 was considered statistically significant.

3. RESULTS

3.1. Scaffold Preparation. A schematic of the scaffold preparation process is illustrated in Figure 1. The process can be divided into three main steps: (1) macromer synthesis and photo-cross-linkable hydrogel preparation, (2) 3D printing of hydrogel, (3) lyophilization. The macromers, including GelMA and HAMA, were synthesized according to their chemical reactions (the binding of methacrylate groups to the primary NH_2 groups of gelatin and the hydroxyl groups of hyaluronic acid, respectively; Figure 1A,B). According to ^1H NMR spectra analysis, after adding MA into gelatin, the lysine signal of the gelatin reduced at 2.9 ppm (a) and the methacrylamide vinyl group signal increased at 5.4 and 5.6 ppm (b), indicating successful MA modification of the gelatin (Figure 2A). Similarly, after adding MA into hyaluronic acid, the N -acetyl glucosamine signal of hyaluronic acid reduced at 1.9 ppm (c) and the methacrylamide vinyl group signal increased at 5.6 and 6.1 ppm (d), indicating successful MA modification of hyaluronic acid (Figure 2B). The viscosity and shear-thinning behavior showed that the viscosity of gel precursor based on GelMA and HAMA decreased as the shear rate increased (Figure 2D). The shear-thinning nature indicated its extrudable property and good printability as the bioink. After exposure to blue light, ^1H NMR spectra analysis showed that the signals of gel precursor distinctly decreased at 1.8–2.5 ppm and 5.4–7.8 ppm, indicating successful

polymerization of GelMA and HAMA (Figure 2C). Dynamic rheology tests showed the fast gelation at approximately 4 s, indicating excellent photocuring performance of gel precursor (Figure 2E). On account of the above shear-thinning nature and fast gelation, gel precursor achieved smooth extrusion and rapid photocuring during 3D printing, which further ensured the outer shape and pore structure maintenance of the 3D-printed hydrogel. After lyophilization, the scaffolds exhibited higher mechanical strength (data not shown) and accurately maintained the original outer shape and pore structure according to macroscopic evaluation (Figure 1E).

Using these methods, accurate human ear- and nose-shaped hydrogel scaffolds were successfully prepared. Likewise, the mechanical strength of ear- and nose-shaped scaffolds was significantly enhanced after lyophilization (data not shown). Importantly, the scaffolds accurately maintained their ear and nose shapes (Figure 3A1–C1, A2–C2) with similarity levels of over 90% compared with the original digital models (Figure 3A1, D1 and E1; A2, D2 and E2). These results further indicated that the novel method established in this study was especially suitable for the fabrication of natural scaffolds with accurate, complex, and defined outer shapes.

3.2. Characterization and Biocompatibility Evaluation of 3D Scaffolds.

3.2.1. Structure Properties of the Lyophilized Scaffolds. Surface morphology and pore structure of the scaffolds were examined by SEM. The surface of the scaffolds exhibited different pore structures at different infill densities and pore size significantly decreased with increased infill density (Figure 4A1–A3, 5A). Noticeably, when the infill density increased to 70%, the hydrogel failed to maintain its accurate pore structure during photocuring 3D printing, probably because of excessive hydrogel and inadequate photocuring speed, which led to low porosity in the lyophilized scaffolds.

3.2.2. Cell Seeding Efficiency, Viability, and Proliferation in the Scaffolds. Cell seeding efficiency was analyzed to evaluate cell adherence within the scaffolds at different infill densities. The results showed that the 50% infill density group achieved the highest cell seeding efficiency at 24 h among all the groups (Figure 5B), which was likely attributed to the optimal pore size and porosity. At day 4 of *in vitro* culture, scaffold pores in 50%

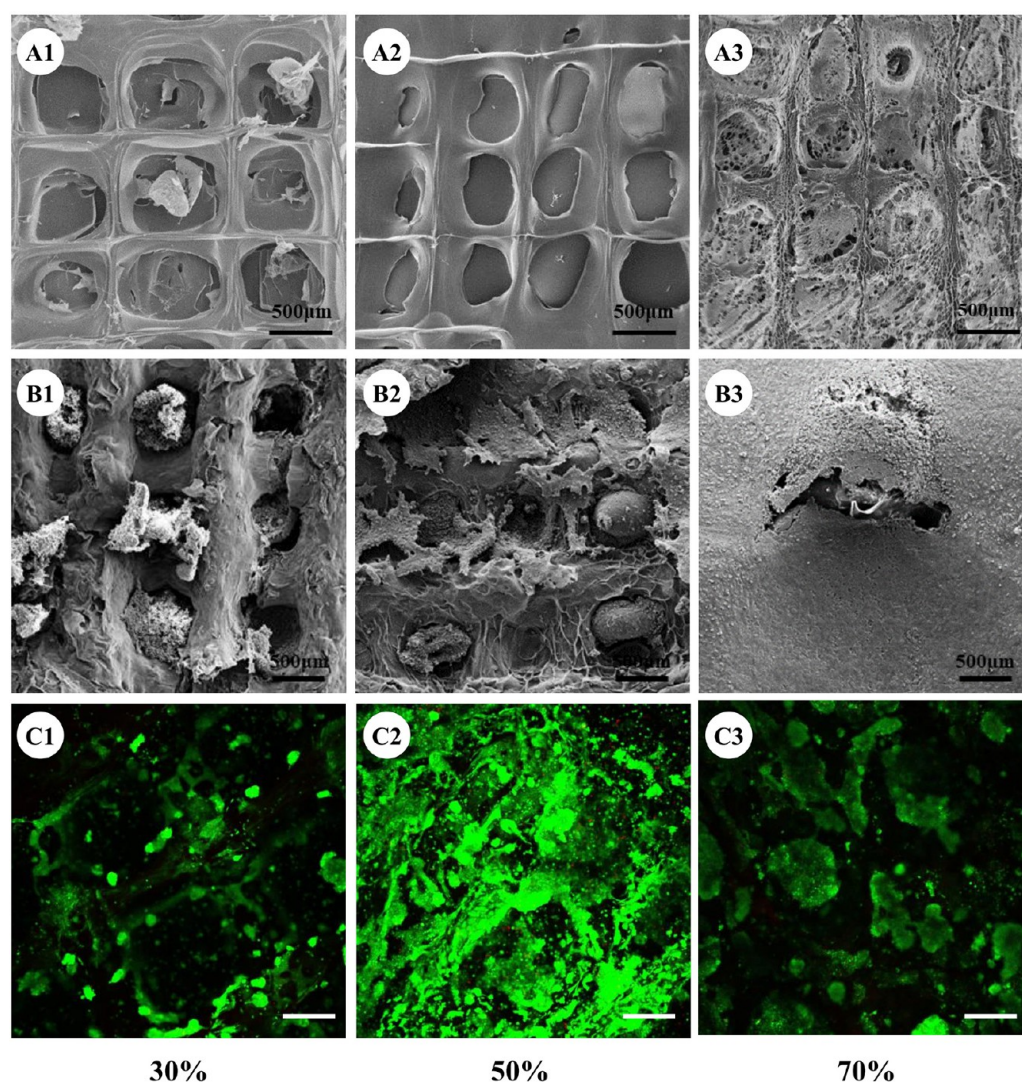


Figure 4. Structure properties and biocompatibility of 3D-printed scaffolds in different infill density groups. The surface of the scaffolds presents different pore structures in the different groups with pore size significantly decreasing with increased infill density (A1–A3). The scaffold in the 70% group fails to maintain an accurate pore structure (A3). SEM and Live & Dead staining show that after cell seeding and 4 days of *in vitro* culture, pore structures in the 50% and 70% groups but not in 30% group were well-filled with chondrocytes and ECM (B1–B3).

and 70% infill density groups were almost completely filled with chondrocytes and ECM, while pores in the 30% group had inadequate coverage (Figure 4B1–B3). Fluorescence micrographs of live/dead staining showed that the majority of chondrocytes were able to effectively adhere to and survive within the scaffolds in all groups, indicating good scaffold biocompatibility and low cytotoxicity (Figure 4C1–C3). Consistent with SEM, the 50% and 70% infill density groups exhibited relatively uniform cell distribution on the surface of the scaffolds; however, the majority of pores in the 30% group were not filled because of excessive pore size. The cell proliferation test showed that the 50% infill density group achieved the highest total DNA content at 1, 4, 7 days among all the groups (Figure 5C), which was consistent with cell seeding efficiency. These results indicated that the 50% infill density group was most appropriate for cell seeding, viability, and proliferation and was therefore chosen as the optimal scaffold for subsequent study.

3.2.3. Scaffold Mechanical and Degradation Tests. Mechanical tests showed that compressive strength and Young's modulus were significantly higher in the lyophilized scaffold than in the 3D-printed hydrogel, with about 3-fold and 5-fold

enhancement, respectively. This indicated that lyophilization could remarkably improve the mechanical properties of the photocured 3D-printed hydrogel scaffolds (Figure 5D,E). Interestingly, after rehydration, the scaffolds retained higher compressive strength and Young's modulus compared with the hydrogel scaffold, with a similar 2.5-fold and 3.5-fold enhancement, respectively (Figure 5D,E). This suggests that the mechanical properties enhanced by lyophilization might be retained during cell seeding and *in vitro* culture. Noticeably, after lyophilization, the *in vitro* degradation time of the scaffolds was prolonged to 8 weeks (the *in vitro* degradation time of 3D-printed hydrogel only reached 4 weeks), more properly matched to cartilage regeneration (Figure 5F).

3.3. In Vitro Cartilage Regeneration. Despite the above promising potential, whether the scaffolds are suitable for cartilage regeneration is still uncertain. The feasibility of cartilage regeneration using our approach was then explored *in vitro* using the lyophilized scaffolds (Figure 6). After cell seeding, the cell-scaffold constructs retained their original shape and gradually formed cartilage-like tissues with increased *in vitro* culture time (Figure 6A1–C1). Histological examination showed that

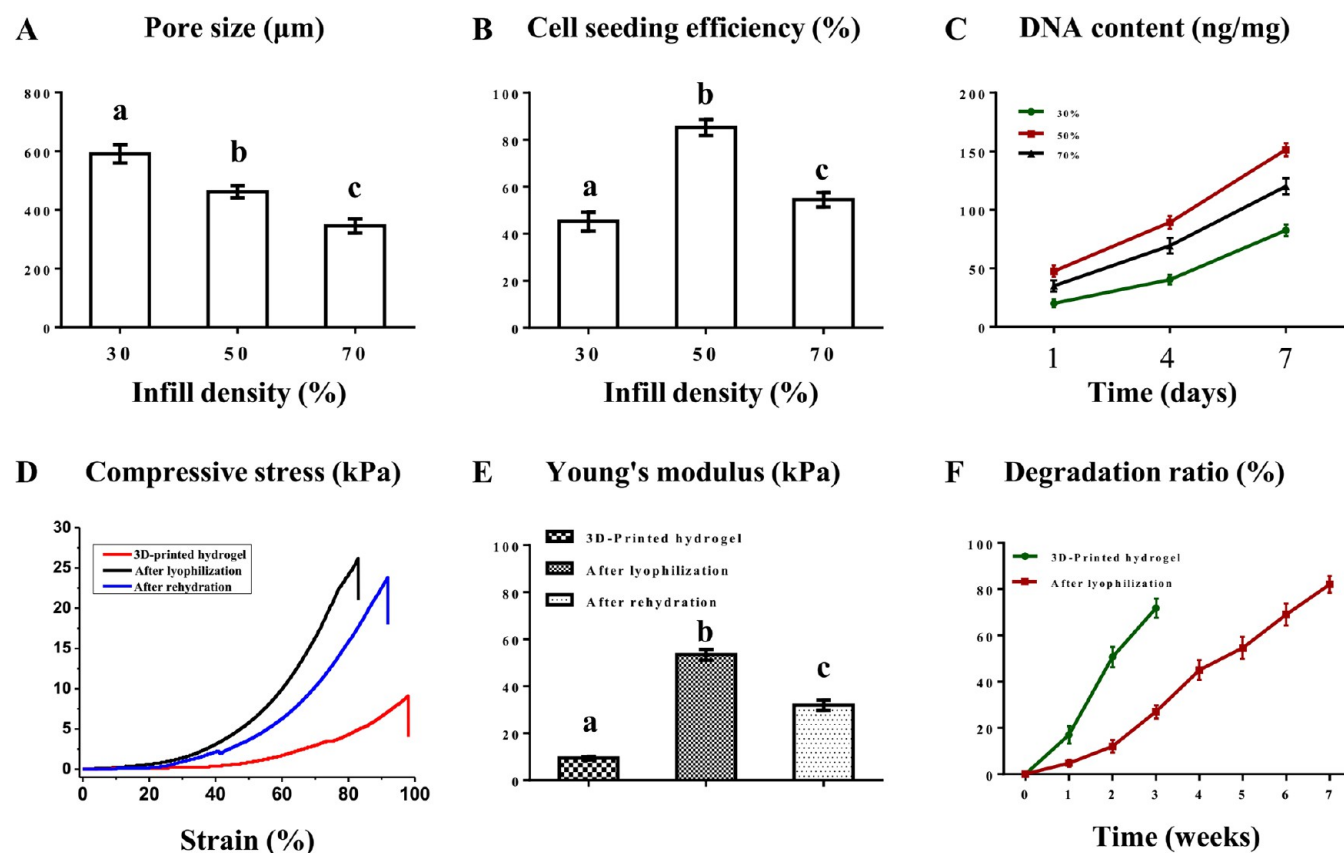


Figure 5. Quantitative analyses on scaffold biocompatibility and characterization. Pore size significantly decreases with increased infill density (A). The 50% group achieves the highest cell-seeding efficiency at 24 h among all the groups (B). DNA quantity presents a similar increase trend in all groups (C). Mechanical tests show that the compressive strength (D) and Young's modulus (E) of the lyophilized scaffolds are significantly higher than those of the 3D-printed hydrogel. After rehydration, the scaffolds retain higher mechanical strength compared with the 3D-printed hydrogel (D,E). The *in vitro* degradation time of the scaffolds is prolonged to 8 weeks after lyophilization while the 3D-printed hydrogel was only maintained to 4 weeks (F).

preliminary cartilage-like tissue was formed at 2 weeks, displaying typical lacunae structures and cartilage-specific ECM deposition (Figure 6A2–A5). Consistent with the macroscopic characteristics, the engineered cartilage matured with the increased *in vitro* culture time, accompanied by gradual degradation of the scaffolds (Figure 6). Biochemical and biomechanical analysis revealed that total collagen, GAG content and mechanical properties of the *in vitro*-engineered cartilage-like tissue also obviously increased over time (Figure 7). These results indicated that the scaffolds were suitable for *in vitro* cartilage regeneration.

3.4. In Vivo Cartilage Regeneration. *In vivo* cartilage regeneration, especially in a large animal model, is the most important evidence for predicting the feasibility of future clinical application. The *in vitro*-engineered cartilage at 2, 4, and 8 weeks was implanted into nude mice for another 8 weeks to evaluate the feasibility of *in vivo* cartilage regeneration. Both histological and quantitative analyses demonstrated that all the resulting *in vitro* engineered cartilage samples matured over time, indicated by increased cartilage ECM deposition and higher mechanical properties (Figures 7 and 8A–C). In particular, the 2-week *in vitro* samples achieved the most satisfactory cartilage regeneration *in vivo*, indicating 2 weeks as a suitable *in vitro* culture time frame prior to *in vivo* implantation (Figure 7A1–A5). To confirm this further, 2-week precultured specimens were subcutaneously implanted into an autologous goat model. The gross view and histological examinations at 8 weeks *in vivo* showed that cartilage-like tissue was steadily regenerated, with

no obvious inflammatory reaction observed. The cartilage-like tissue further matured with typical cartilage features and abundant ECM deposition (Figure 9), predicting promising potential in clinical application.

4. DISCUSSION

Native polymers, such as gelatin and hyaluronic acid, have become favorable biomimetic scaffold sources for cartilage regeneration. However, the precise control of their structure, degradation rate, and mechanical properties remains challenging. These issues were addressed in the current study by fabricating gelatin and hyaluronic acid into a photo-cross-linkable hydrogel prior to their creation into precise shapes with good internal pore structures via a photocuring 3D printing technique. Moreover, the hydrogel scaffolds were lyophilized to improve their mechanical strength and slow their degradation rate. Most importantly, tissue-engineered cartilage with typical lacunae structures and cartilage-specific ECM was successfully regenerated from chondrocyte–scaffold constructs both *in vitro* and *in vivo*, indicating promising application of these scaffolds in cartilage regeneration.

Developing methods to precisely control the outer shape and internal pore structure is a primary problem using gelatin- and hyaluronic acid-based scaffolds for cartilage regeneration. Lyophilization is the most common method used to date.^{35–37} However, with this approach it is difficult to achieve unique and highly complex outer shapes as well as precisely control the internal structures (pore size, orientation, and connectivity).

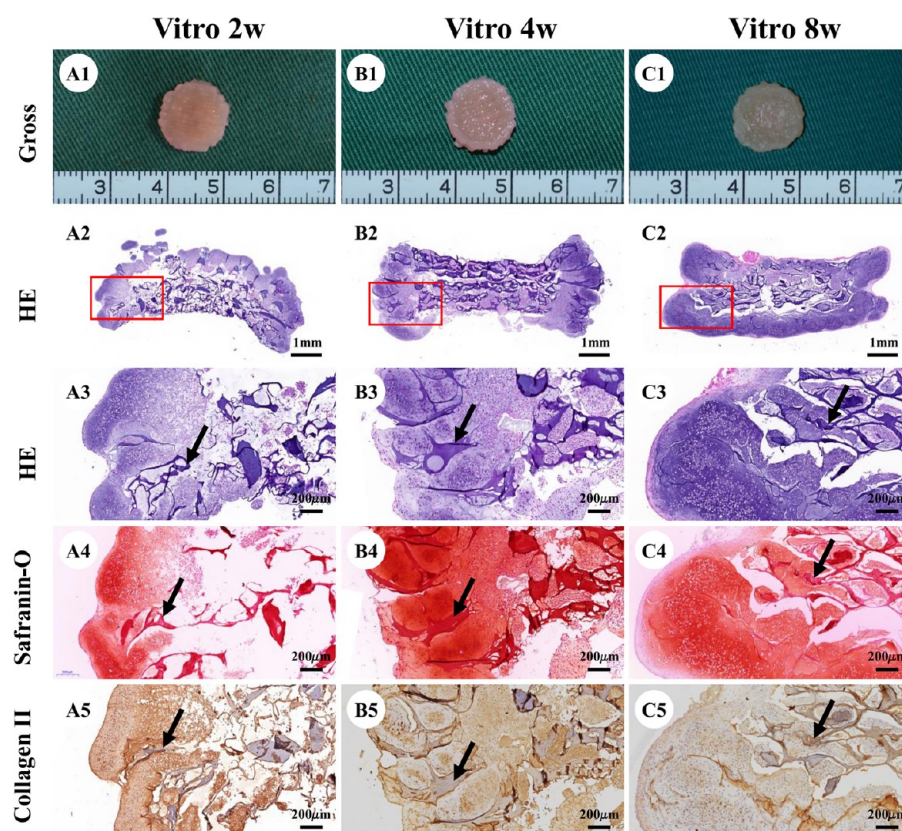


Figure 6. Gross view and histological examinations of *in vitro* engineered cartilage. After cell seeding, all samples at 2, 4, and 8 weeks retain their original shape and form cartilage-like tissues with a gradually matured cartilage appearance (A1–C1). Histologically, the engineered cartilage is preliminarily formed at 2 weeks with typical lacunae structures and cartilage-specific ECM deposition (A2–A5) and matures with increased *in vitro* culture time accompanied by gradual degradation of the scaffolds (A–C) (black arrows indicate residual scaffold).

Three-dimensional printing can achieve precise digital control of the outer shape and the internal porosity via spatially- and temporally-controlled deposition using computer-aided design/computer-aided manufacturing (CAD/CAM) technology and thus provides a better solution for structure control.^{38–40} Similar to other native polymers, gelatin and hyaluronic acid have to be printed in the form of a hydrogel, thus we need to resolve the problem of curing during 3D printing to maintain their precise structure. Thermosensitive and photo-cross-linkable hydrogels are the most commonly used gelatin and hyaluronic acid forms for 3D printing, because their sol–gel transition characteristic ensures smooth extrusion and structure maintenance during the process.^{41–44} For thermosensitive hydrogels, the precise outer shape and internal pore structure are easily affected by temperature change and the second-step cross-linking after 3D printing, while photo-cross-linkable hydrogels may overcome this deficiency because 3D printing and the cross-linking reaction can be achieved in one step.^{43,44} Consequently, a photo-cross-linkable hydrogel was applied for 3D printing in the current study.

In the current study, human ear- and nose-shaped hydrogels and their lyophilized scaffolds were successfully prepared based on a photo-cross-linkable hydrogel, and both scaffolds achieved similarity levels over 90% compared with the original digital models, indicating that photocuring 3D printing was especially suitable for fabrication of the natural scaffolds with an accurate, complex, and unique outer shape.

How to control scaffold pore size for optimal cartilage regeneration is also a challenge.^{45,46} Large pore size may lead to excessive cell leakage and inefficient cell adhesion, while small

pore size may render cells to accumulate on the surface of the scaffold, resulting in heterogeneous cell distribution and inferior internal nutrition supply.⁴⁷ However, it remains unclear what parameters during 3D printing are appropriate for chondrocyte adherence and proliferation and subsequent cartilage regeneration. To address this issue, the current study optimized the scaffold pore size by adjusting the filling rate parameters during 3D printing. The results showed that scaffolds with a 50% infill density had higher cell seeding efficiency and more homogeneous cell distribution compared with 30% and 70% groups. Therefore, scaffolds prepared with this parameter were used for subsequent experiments.

Poor mechanical properties and excessive degradation rate are two other major problems for gelatin- and hyaluronic acid-based scaffolds in cartilage regeneration. The photo-cross-linking reaction in the current system improved the mechanical strength and slowed the degradation rate to some extent.^{48,49} Nevertheless, the mechanical and *in vitro* degradation tests showed that both the maximum compressive strength and Young's modulus of the 3D-printed hydrogel only achieved about 10 kPa, and the *in vitro* degradation time was maintained for approximately 4 weeks (Figure 4D–F), which is inadequate for cartilage regeneration.^{25,50} Lyophilization can transform the 3D-printed hydrogel from gel state to a more stable solid state. During lyophilization, dehydration contributed to more compact network with shorter distance and stronger interaction forces between macromolecules, which further improved the mechanical strength and degradation rate of the lyophilized scaffolds. Due to the compact and strong network, the lyophilized

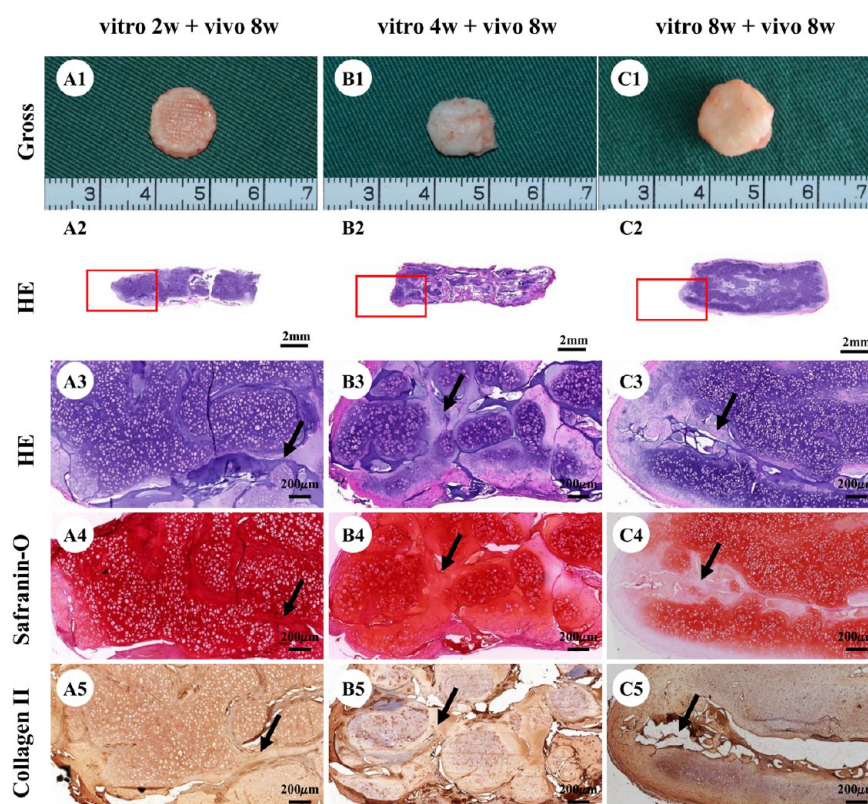


Figure 7. Gross view and histological examinations of the regenerated cartilage in nude mice. After 8 weeks of *in vivo* implantation, all samples from weeks 2, 4, and 8 *in vitro* successfully regenerate relatively homogeneous mature cartilage with typical lacunae structures and cartilage-specific ECM deposition (A–C). Minimal residual scaffold is still observed (black arrows indicate residual scaffold).

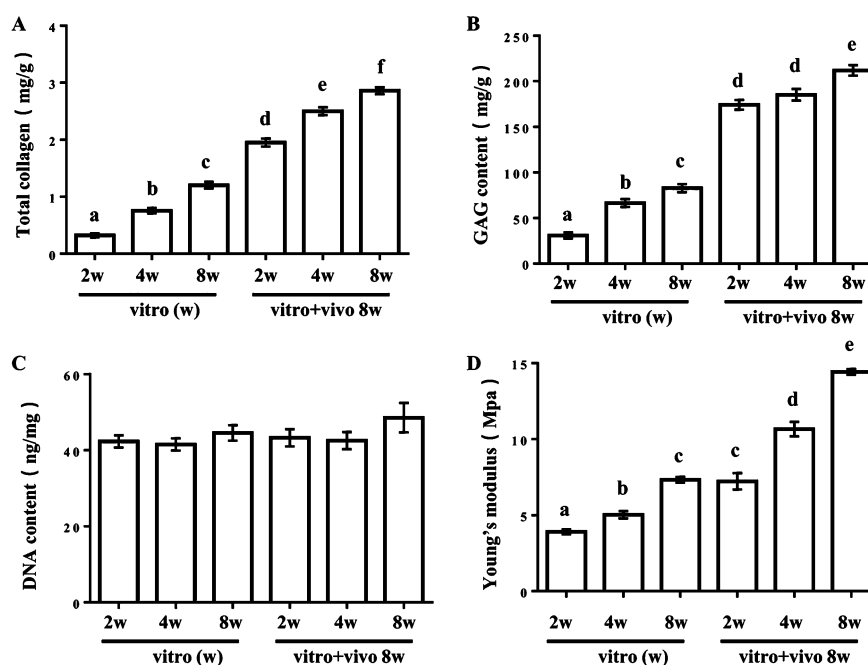


Figure 8. Quantitative evaluations of the regenerated cartilage *in vitro* and in nude mice. Total collagen (A), GAG content (B), and Young's modulus (C) of *in vitro*-engineered cartilage increased with increased *in vitro* culture time. After 8 weeks of implantation in nude mice, all the above quantitative data are significantly enhanced compared with the corresponding *in vitro* groups (A–C). No significant differences are observed in the DNA quantification among groups (D).

scaffolds after rehydration retained their structure and mechanical strength to a great extent rather than recover to its initial state before lyophilization. This may be the molecular mechanism that the lyophilized scaffolds before and after

rehydration had stronger mechanical strength and lower degradation rate compared to the 3D printed hydrogel. The results demonstrated that the maximum compressive strength and Young's modulus of the scaffolds after lyophilization

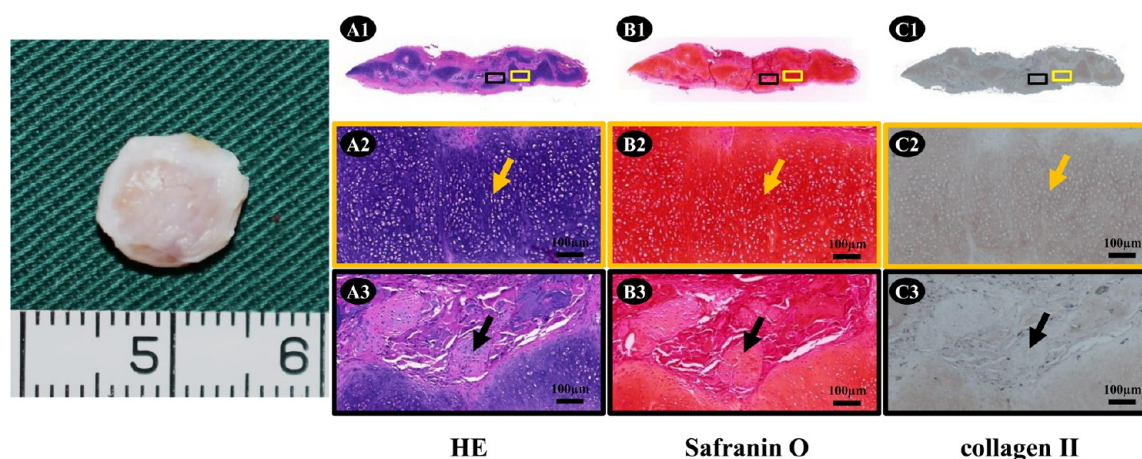


Figure 9. Gross view and histological examinations of the regenerated cartilage in an autologous goat. After 8 weeks of autologous implantation in the goat, 2-week *in vitro* samples successfully regenerate relatively homogeneous mature cartilage with typical lacuna structures and cartilage-specific ECM deposition (A–C). No obvious inflammatory infiltration is observed between the regenerated cartilage and surrounding native tissue (Yellow arrows indicate mature cartilage; black arrows indicate newly regenerated cartilage with the degradation of scaffolds).

increased about 3-fold and 5-fold, respectively. Simultaneously, the *in vitro* degradation time was prolonged to approximately 8 weeks, which more properly matched to cartilage regeneration. These results indicated that lyophilization enhanced mechanical strength of the 3D-printed hydrogel and slowed its degradation rate. After lyophilization, the scaffolds also had the following advantages: (i) more favorable cell seeding and adherence owing to superior water absorbability; (ii) more convenient operation owing to higher mechanical strength; (iii) more convenient sterilization, storage, and transportation with greater potential for productization.

Despite the significant improvement in pore structure, mechanical strength, and degradation rate, whether the current scaffolds could achieve satisfactory cartilage regeneration was concerning. The results showed that chondrocytes could adhere to, survive within, and proliferate effectively in the scaffolds. Moreover, engineered cartilage with typical lacunae structure and cartilage-specific ECM was successfully regenerated both *in vitro* and *in vivo*. Noticeably, cartilage-like tissue was successfully regenerated within 2 weeks *in vitro*, which was faster than cartilage regeneration using polyglycolic acid/polyglycolic acid (PLA/PGA) scaffolds (about 4–8 weeks).²⁵ Most importantly, the 2-week *in vitro*-engineered cartilage could successfully regenerate stable mature cartilage in immunocompetent large animals with no obvious inflammatory reaction observed, despite showing abundant residual scaffold. This finding indicates that 2 weeks of *in vitro* culture is optimal for the current scaffolds to permit autologous *in vivo* cartilage regeneration in future clinical application, which could greatly decrease associated patient treatment costs and waiting times. Interestingly, synthesized polymers, such as PLA/PGA, are reported to trigger inflammatory reactions and lead to cartilage regeneration failure in immunocompetent large animals and humans.²⁵ Consequently, our previous clinical application of ear-shaped cartilage based on PLA/PGA scaffolds required >12 weeks of *in vitro* culture to avoid *in vivo* inflammatory reactions to achieve satisfactory cartilage regeneration and auricular reconstruction.⁵⁰

Favorable cartilage regeneration *in vitro* and *in vivo* may attribute to the following aspects: (i) good biocompatibility of gelatin and hyaluronic acid as the component of native cartilage ECM; (ii) optimal pore structure controlled by photocuring 3D printing and lyophilization suitable for cell distribution and nutrient supply;

(iii) superior water-absorbing capacity, high mechanical strength, and optimal degradation rate for cell-seeding and cartilage regeneration; (iv) weak immunogenicity and low cytotoxicity avoiding an inflammatory reaction to permit stable cartilage regeneration in goats. All these factors contribute to satisfactory cartilage regeneration both *in vitro* and *in vivo*.

In summary, the current study has demonstrated that photo-cross-linkable gelatin and hyaluronic acid can be fabricated as a porous scaffold with a precise outer shape, good internal pore structure, high mechanical strength, and good degradation rate, through photocuring 3D printing and lyophilization. The scaffolds combined with chondrocytes successfully regenerated mature cartilage with typical lacunae structure and cartilage-specific ECM both *in vitro* and *in vivo*. Although mechanical strength of the scaffolds warrants further enhancement, and the feasibility of regenerating precisely shaped cartilage needs to be further explored *in vitro* and *in vivo*, the current study provides a novel strategy for porous scaffold fabrication based on native polymers and a novel biodegradable scaffold with satisfactory outer shape, pore structure, mechanical strength, degradation rate, and weak immunogenicity for cartilage regeneration.

AUTHOR INFORMATION

Corresponding Authors

*Phone: +86-21-23271699 ext. 5192. Fax: +86-21-53078128.

E-mail: guangdongzhou@126.com.

*E-mail: huimin.chen@stemeasy.com.

*E-mail: gaokongliuyun@126.com.

ORCID

Guangdong Zhou: 0000-0003-2488-2733

Author Contributions

[§]H.X., D.Z., H.Z., and Y.H. contributed equally to this work.

Notes

The authors declare no competing financial interest.

ACKNOWLEDGMENTS

This work was supported by the National Natural Science Foundation of China (Grants 81571823, 81771568, 31700837, and 81701843), The National Key Research and Development Program of China (Grant 2017YFC1103900), The Key Research and Development Program of Shandong Province

(Grant 2016GGB14002), Jiangsu Provincial Key Research and Development Program (BE2016010-2), the Shanghai Committee of Science and Technology (Grant 15DZ1941600), the Program of Shanghai Technology Research Leader, and the Program for Shanghai Outstanding Medical Academic Leader. We thank Elizabeth Finnie, Ph.D., from Edanz Group (www.edanzediting.com/ac) for editing a draft of this manuscript.

REFERENCES

- (1) Setton, L. A.; Elliott, D. M.; Mow, V. C. Altered mechanics of cartilage with osteoarthritis: human osteoarthritis and an experimental model of joint degeneration. *Osteoarthritis Cartilage* **1999**, *7* (1), 2.
- (2) Jackson, D. W.; Scheer, M. J.; Simon, T. M. Cartilage substitutes: overview of basic science and treatment options. *J. Am. Acad. Orthop Surg* **2001**, *9* (1), 37.
- (3) Wigganhauser, P. S.; Schantz, J. T.; Rotter, N. Cartilage engineering in reconstructive surgery: auricular, nasal and tracheal engineering from a surgical perspective. *Regener. Med.* **2017**, *12* (3), 303–314.
- (4) Langer, R.; Vacanti, J. P. Tissue engineering. *Science* **1993**, *260* (5110), 920.
- (5) Raghunath, J.; Rollo, J.; Sales, K. M.; Butler, P. E.; Seifalian, A. M. Biomaterials and scaffold design: key to tissue-engineering cartilage. *Biotechnol. Appl. Biochem.* **2007**, *46* (2), 73–84.
- (6) Vinatier, C.; Mrugala, D.; Jorgensen, C.; Guicheux, J.; Noel, D. Cartilage engineering: a crucial combination of cells, biomaterials and biofactors. *Trends Biotechnol.* **2009**, *27* (5), 307.
- (7) Filardo, G.; Kon, E.; Roffi, A.; Di Martino, A.; Marcacci, M. Scaffold-based repair for cartilage healing: a systematic review and technical note. *Arthroscopy* **2013**, *29* (1), 174–86.
- (8) Gunatillake, P. A.; Adhikari, R. Biodegradable synthetic polymers for tissue engineering. *Eur. Cell Mater.* **2003**, *5*, 1–16.
- (9) Yao, Q.; Wei, B.; Liu, N.; Li, C.; Guo, Y.; Shamie, A. N.; Chen, J.; Tang, C.; Jin, C.; Xu, Y.; Bian, X.; Zhang, X.; Wang, L. Chondrogenic regeneration using bone marrow clots and a porous polycaprolactone-hydroxyapatite scaffold by three-dimensional printing. *Tissue Eng., Part A* **2015**, *21* (7–8), 1388–97.
- (10) Rao, S. H.; Harini, B.; Shadamarshan, R. P. K.; Balagangadharan, K.; Selvamurugan, N. Natural and synthetic polymers/bioceramics/bioactive compounds-mediated cell signalling in bone tissue engineering. *Int. J. Biol. Macromol.* **2018**, *110*, 88–96.
- (11) Dang, J. M.; Leong, K. W. Natural polymers for gene delivery and tissue engineering. *Adv. Drug Delivery Rev.* **2006**, *58* (4), 487–99.
- (12) Liu, M.; Zeng, X.; Ma, C.; Yi, H.; Ali, Z.; Mou, X.; Li, S.; Deng, Y.; He, N. Injectable hydrogels for cartilage and bone tissue engineering. *Bone Res.* **2017**, *5*, 17014.
- (13) Sengupta, D.; Heilshorn, S. C. Protein-engineered biomaterials: highly tunable tissue engineering scaffolds. *Tissue Eng., Part B* **2010**, *16* (3), 285–93.
- (14) Fan, H.; Hu, Y.; Zhang, C.; Li, X.; Lv, R.; Qin, L.; Zhu, R. Cartilage regeneration using mesenchymal stem cells and a PLGA-gelatin/chondroitin/hyaluronate hybrid scaffold. *Biomaterials* **2006**, *27* (26), 4573–80.
- (15) Muzzarelli, R. A.; Greco, F.; Busilacchi, A.; Sollazzo, V.; Gigante, A. Chitosan, hyaluronan and chondroitin sulfate in tissue engineering for cartilage regeneration: a review. *Carbohydr. Polym.* **2012**, *89* (3), 723–39.
- (16) Li, L.; He, Z. Y.; Wei, X. W.; Wei, Y. Q. Recent advances of biomaterials in biotherapy. *Regen Biomater* **2016**, *3* (2), 99–105.
- (17) Little, C. J.; Bawolin, N. K.; Chen, X. Mechanical properties of natural cartilage and tissue-engineered constructs. *Tissue Eng., Part B* **2011**, *17* (4), 213–27.
- (18) Li, J.; Chen, M.; Fan, X.; Zhou, H. Recent advances in bioprinting techniques: approaches, applications and future prospects. *J. Transl. Med.* **2016**, *14*, 271.
- (19) Faramarzi, N.; Yazdi, I. K.; Nabavinia, M.; Gemma, A.; Fanelli, A.; Caizzone, A.; Ptaszek, L. M.; Sinha, I.; Khademhosseini, A.; Ruskin, J. N. Patient-Specific Bioinks for 3D Bioprinting of Tissue Engineering Scaffolds. *Adv. Healthcare Mater.* **2018**, *7* (11), 1870043.
- (20) Bédouet, A.; Piacentini, N.; Aeberli, L.; Da Silva, A.; Verheyen, C. A.; Bonini, F.; Rochat, A.; Filippova, A.; Serex, L.; Renaud, P.; Braschler, T. Additive manufacturing of hierarchical injectable scaffolds for tissue engineering. *Acta Biomater.* **2018**, *76*, 71.
- (21) Levett, P. A.; Melchels, F. P.; Schrobback, K.; Huttmacher, D. W.; Malda, J.; Klein, T. J. A biomimetic extracellular matrix for cartilage tissue engineering centered on photocurable gelatin, hyaluronic acid and chondroitin sulfate. *Acta Biomater.* **2014**, *10* (1), 214–23.
- (22) Gaetani, R.; Feyen, D. A.; Verhage, V.; Slaats, R.; Messina, E.; Christman, K. L.; Giacomello, A.; Doevendans, P. A.; Sluijter, J. P. Epicardial application of cardiac progenitor cells in a 3D-printed gelatin/hyaluronic acid patch preserves cardiac function after myocardial infarction. *Biomaterials* **2015**, *61*, 339–48.
- (23) Nichol, J. W.; Koshy, S. T.; Bae, H.; Hwang, C. M.; Yamanlar, S.; Khademhosseini, A. Cell-laden microengineered gelatin methacrylate hydrogels. *Biomaterials* **2010**, *31* (21), 5536–44.
- (24) Smeds, K. A.; Pfister-Serres, A.; Miki, D.; Dastgheib, K.; Inoue, M.; Hatchell, D. L.; Grinstaff, M. W. Photocrosslinkable polysaccharides for in situ hydrogel formation. *J. Biomed Mater. Res.* **2001**, *54* (1), 115–121.
- (25) Liu, Y.; Zhang, L.; Zhou, G.; Li, Q.; Liu, W.; Yu, Z.; Luo, X.; Jiang, T.; Zhang, W.; Cao, Y. In vitro engineering of human ear-shaped cartilage assisted with CAD/CAM technology. *Biomaterials* **2010**, *31* (8), 2176–83.
- (26) Liu, Y.; Li, D.; Yin, Z.; Luo, X.; Liu, W.; Zhang, W.; Zhang, Z.; Cao, Y.; Liu, Y.; Zhou, G. Prolonged in vitro precultivation alleviates post-implantation inflammation and promotes stable subcutaneous cartilage formation in a goat model. *Biomed Mater.* **2017**, *12* (1), 015006.
- (27) Zheng, R.; Duan, H.; Xue, J.; Liu, Y.; Feng, B.; Zhao, S.; Zhu, Y.; Liu, Y.; He, A.; Zhang, W.; Liu, W.; Cao, Y.; Zhou, G. The influence of Gelatin/PCL ratio and 3-D construct shape of electrospun membranes on cartilage regeneration. *Biomaterials* **2014**, *35* (1), 152–64.
- (28) Yang, Y.; Zhang, J.; Liu, Z.; Lin, Q.; Liu, X.; Bao, C.; Wang, Y.; Zhu, L. Tissue-Integratable and Biocompatible Photogelation by the Imine Crosslinking Reaction. *Adv. Mater.* **2016**, *28* (14), 2724–30.
- (29) Chen, W.; Chen, S.; Morsi, Y.; El-Hamshary, H.; El-Newhy, M.; Fan, C.; Mo, X. Superabsorbent 3D Scaffold Based on Electrospun Nanofibers for Cartilage Tissue Engineering. *ACS Appl. Mater. Interfaces* **2016**, *8* (37), 24415–25.
- (30) Wang, S.; Guan, S.; Zhu, Z.; Li, W.; Liu, T.; Ma, X. Hyaluronic acid doped-poly(3,4-ethylenedioxythiophene)/chitosan/gelatin (PEDOT-HA/Cs/Gel) porous conductive scaffold for nerve regeneration. *Mater. Sci. Eng., C* **2017**, *71*, 308–316.
- (31) He, A.; Xia, H.; Xiao, K.; Wang, T.; Liu, Y.; Xue, J.; Li, D.; Tang, S.; Liu, F.; Wang, X.; Zhang, W.; Liu, W.; Cao, Y.; Zhou, G. Cell yield, chondrogenic potential, and regenerated cartilage type of chondrocytes derived from ear, nasoseptal, and costal cartilage. *J. Tissue Eng. Regen. Med.* **2018**, *12* (4), 1123–1132.
- (32) Li, D.; Zhu, L.; Liu, Y.; Yin, Z.; Liu, Y.; Liu, F.; He, A.; Feng, S.; Zhang, Y.; Zhang, Z.; Zhang, W.; Liu, W.; Cao, Y.; Zhou, G. Stable subcutaneous cartilage regeneration of bone marrow stromal cells directed by chondrocyte sheet. *Acta Biomater.* **2017**, *54*, 321–332.
- (33) Chen, J.; Yuan, Z.; Liu, Y.; Zheng, R.; Dai, Y.; Tao, R.; Xia, H.; Liu, H.; Zhang, Z.; Zhang, W.; Liu, W.; Cao, Y.; Zhou, G. Improvement of In Vitro Three-Dimensional Cartilage Regeneration by a Novel Hydrostatic Pressure Bioreactor. *Stem Cells Transl. Med.* **2017**, *6* (3), 982–991.
- (34) Zhang, Y.; Yang, F.; Liu, K.; Shen, H.; Zhu, Y.; Zhang, W.; Liu, W.; Wang, S.; Cao, Y.; Zhou, G. The impact of PLGA scaffold orientation on in vitro cartilage regeneration. *Biomaterials* **2012**, *33* (10), 2926–35.
- (35) Offeddu, G. S.; Ashworth, J. C.; Cameron, R. E.; Oyen, M. L. Structural determinants of hydration, mechanics and fluid flow in freeze-dried collagen scaffolds. *Acta Biomater.* **2016**, *41*, 193–203.

- (36) Yu, X.; Qian, G.; Chen, S.; Xu, D.; Zhao, X.; Du, C. A tracheal scaffold of gelatin-chondroitin sulfate-hyaluronan-polyvinyl alcohol with orientated porous structure. *Carbohydr. Polym.* **2017**, *159*, 20–28.
- (37) Wu, X.; Liu, Y.; Li, X.; Wen, P.; Zhang, Y.; Long, Y.; Wang, X.; Guo, Y.; Xing, F.; Gao, J. Preparation of aligned porous gelatin scaffolds by unidirectional freeze-drying method. *Acta Biomater.* **2010**, *6* (3), 1167–77.
- (38) Liu, X.; Yuk, H.; Lin, S.; Parada, G. A.; Tang, T. C.; Tham, E.; de la Fuente-Nunez, C.; Lu, T. K.; Zhao, X. 3D Printing of Living Responsive Materials and Devices. *Adv. Mater.* **2018**, *30* (4), 1870021.
- (39) Wang, X.; Wei, C.; Cao, B.; Jiang, L.; Hou, Y.; Chang, J. Fabrication of Multiple-Layered Hydrogel Scaffolds with Elaborate Structure and Good Mechanical Properties via 3D Printing and Ionic Reinforcement. *ACS Appl. Mater. Interfaces* **2018**, *10* (21), 18338–18350.
- (40) Nagarajan, N.; Dupret-Bories, A.; Karabulut, E.; Zorlutuna, P.; Vrana, N. E. Enabling personalized implant and controllable biosystem development through 3D printing. *Biotechnol. Adv.* **2018**, *36* (2), 521–533.
- (41) Roehm, K. D.; Madihally, S. V. Bioprinted chitosan-gelatin thermosensitive hydrogels using an inexpensive 3D printer. *Biofabrication* **2018**, *10* (1), 015002.
- (42) Abbadessa, A.; Mouser, V. H. M.; Blokzijl, M. M.; Gawlitta, D.; Dhert, W. J. A.; Hennink, W. E.; Malda, J.; Vermonden, T. A Synthetic Thermosensitive Hydrogel for Cartilage Bioprinting and Its Biofunctionalization with Polysaccharides. *Biomacromolecules* **2016**, *17* (6), 2137–2147.
- (43) Kim, S. H.; Yeon, Y. K.; Lee, J. M.; Chao, J. R.; Lee, Y. J.; Seo, Y. B.; Sultan, M. T.; Lee, O. J.; Lee, J. S.; Yoon, S. I.; Hong, I. S.; Khang, G.; Lee, S. J.; Yoo, J. J.; Park, C. H. Precisely printable and biocompatible silk fibroin bioink for digital light processing 3D printing. *Nat. Commun.* **2018**, *9* (1), 1620.
- (44) Louzao, I.; Koch, B.; Taresco, V.; Ruiz-Cantu, L.; Irvine, D. J.; Roberts, C. J.; Tuck, C.; Alexander, C.; Hague, R.; Wildman, R.; Alexander, M. R. Identification of Novel "Inks" for 3D Printing Using High-Throughput Screening: Bioresorbable Photocurable Polymers for Controlled Drug Delivery. *ACS Appl. Mater. Interfaces* **2018**, *10* (8), 6841–6848.
- (45) Lien, S. M.; Ko, L. Y.; Huang, T. J. Effect of pore size on ECM secretion and cell growth in gelatin scaffold for articular cartilage tissue engineering. *Acta Biomater.* **2009**, *5* (2), 670–9.
- (46) Lewis, P. L.; Green, R. M.; Shah, R. N. 3D-printed gelatin scaffolds of differing pore geometry modulate hepatocyte function and gene expression. *Acta Biomater.* **2018**, *69*, 63–70.
- (47) Zhang, Y.; Yang, F.; Liu, K.; Shen, H.; Zhu, Y.; Zhang, W.; Liu, W.; Wang, S.; Cao, Y.; Zhou, G. The impact of PLGA scaffold orientation on in vitro cartilage regeneration. *Biomaterials* **2012**, *33* (10), 2926–35.
- (48) O'Connell, C. D.; Zhang, B.; Onofriello, C.; Duchi, S.; Blanchard, R.; Quigley, A.; Bourke, J.; Gambhir, S.; Kapsa, R.; Di Bella, C.; Choong, P.; Wallace, G. G. Tailoring the mechanical properties of gelatin methacryloyl hydrogels through manipulation of the photocrosslinking conditions. *Soft Matter* **2018**, *14* (11), 2142–2151.
- (49) Kang, W.; Bi, B.; Zhuo, R.; Jiang, X. Photocrosslinked methacrylated carboxymethyl chitin hydrogels with tunable degradation and mechanical behavior. *Carbohydr. Polym.* **2017**, *160*, 18–25.
- (50) Zhou, G.; Jiang, H.; Yin, Z.; Liu, Y.; Zhang, Q.; Zhang, C.; Pan, B.; Zhou, J.; Zhou, X.; Sun, H.; Li, D.; He, A.; Zhang, Z.; Zhang, W.; Liu, W.; Cao, Y. In Vitro Regeneration of Patient-specific Ear-shaped Cartilage and Its First Clinical Application for Auricular Reconstruction. *EBioMedicine* **2018**, *28*, 287–302.